DRYING TECHNOLOGY, 19(9), 2209–2234 (2001)

A NUMERICAL AND EXPERIMENTAL STUDY OF MICROWAVE DRYING USING A RECTANGULAR WAVE GUIDE

P. Ratanadecho,* K. Aoki, and M. Akahori

Department of Mechanical Engineering, Nagaoka University of Technology, 1603-1, Kamitomioka, Nagaoka, Niigata, 940-2188, Japan

ABSTRACT

The drying of a capillary porous packed bed of glass beads by microwave energy using a rectangular wave-guide was investigated numerically and experimentally. The effects of moisture content, particle size and microwave power level on the drying kinetics were examined. Most importantly, this work focuses on the prediction of the distribution of the electromagnetic field as well as the temperature and moisture distribution within the capillary porous medium. The model, which combines the electromagnetic, temperature, and moisture fields, predicted results which were in good agreement with the experimental data.

Key Words: Electromagnetic field; Reflection; Capillary porous packed bed; Dielectric materials

* Corresponding author. Nagaoka University of Technology, 1603-1, Kamitomioka, Nagaoka, Niigata, 940-2188, Japan. E-mail: phadu@blue.nagaokaut.ac.jp

INTRODUCTION

A convenient starting point of drying theory is a recent work by Whitaker (1977), who derived locally volume averaged conservation equations for two-phase capillary flow in porous media. A practical way to distinguish between the various drying processes is to classify them by the heating mode: convective drying, radiative drying, and conductive drying. Drying with internal heat generation, such as dielectric drying or microwave drying, is a special case. See Mujumdar (1995) for a detailed discussion.

In the past decade, microwave technology has been applied to many processes. Some of the successful examples of this application is in ceramics processing for drying and sintering, drying of paper, freeze drying, and vulcanization of rubber. Refer to Metaxas and Meredith (1983) and Saltiel and Datta (1997) for an introduction to heat and mass transfer in microwave processing.

Simultaneous heat and mass transport in microwave drying was studied by Wei et al. (1985) with the aid of Lambert's law, while Perkin et al. (1980) measured the temperature, moisture content, and pressure profiles in porous materials heated by microwave energy. Intensive microwave drying has been studied by Turner and Jolly (1991), Turner and Ilic (1991), Constant et al. (1996) and Ni et al. (1999). A number of other possible analyses of conventional drying process and application of microwave process have appeared in the literatures (8)–(21).

Most previous work the microwave power absorbed was assumed to decay exponentially into the sample following the aid of Lambert's law. This assumption is valid for the large dimensions of sample used in study. For small samples, the spatial variations of the electromagnetic field and microwave power absorbed within sample must be obtained by a complete solution of the unsteady Maxwell's equations.

Due to the limited amount of theoretical and experimental work on microwave drying of capillary porous materials, the various effects are not fully understood and a number of critical issues remain unresolved. This effects of reflection rate of microwave, degree of incident wave penetration into the sample, particle size and microwave power level during microwave drying process etc. have not been studied systematically.

Although most of previous investigations considered one-dimensional heat and mass transport little effort has been reported on study of two-dimensional drying process by microwave fields, especially, full comparison between mathematical simulation results with experimental drying data. This study reports a comparison of predictions based on a two-dimensional model with experimental measurement in which the microwave of TE_{10} mode operating at a frequency of 2.45 GHz is employed.

Generally the variation of the microwave power level and change of particle size (glass bead size) during microwave drying of capillary porous material could change the degree of penetration and rate of heat generation within the sample. Since the reflection rate of microwave strongly depends on the moisture content of the sample so that the effects of particle size and the variation of microwave power level must be considered in this work. The specific objectives of this work are to

- formulate and solve the generalized mathematical model of drying process by microwaves is purpose;
- compare the numerical results with experimental measurements

EXPERIMENTAL APPARATUS

Figure 1 shows the experimental apparatus used. The MW System was a monochromatic wave of TE_{10} mode operating at a frequency of 2.45 GHz. MW energy is transmitted along the z-direction of the rectangular wave guide with inside dimensions of 109.22 um $\times$ 54.61 mm toward a water load that is situated at the end of the wave guide. The water load (lower absorbing boundary) ensures that only a minimal amount of microwave is reflected back to the sample, while an upper absorbing boundary, which is located at the end of wave guide, is used to trap any microwave reflected from the sample to prevent it from damaging the magnetron. The sample (capillary porous packed bed) studied is an initially saturated rectangular packed bed, which is composed of glass beads and water with a bed thickness of 50 mm. It is inserted in the rectangular wave guide. The container is made of polypropylene of 0.75 mm thickness. The sample porosity and permeability were measured. Dielectric properties of the sample at various conditions were measured (Von Hippel, 1954). During the experiment, the weight of the sample, the ambient temperature, the temperature of the sample at eight locations, the transmitted microwave power, the reflected microwave power, and the microwave power absorbed by the sample were recorded by a data logger that was connected to a computer.

The microwave field was generated using a magnetron (Micro Denshi Co., Model UM-1500). The powers of incident, reflected and transmitted waves were measured by wattmeter using a directional coupler (Micro Denshi Co., model DR-5000). The temperature was measured with a Luxtron fluroptic thermometer model 790 (accurate to $\pm 0.5\,^{\circ}C$).

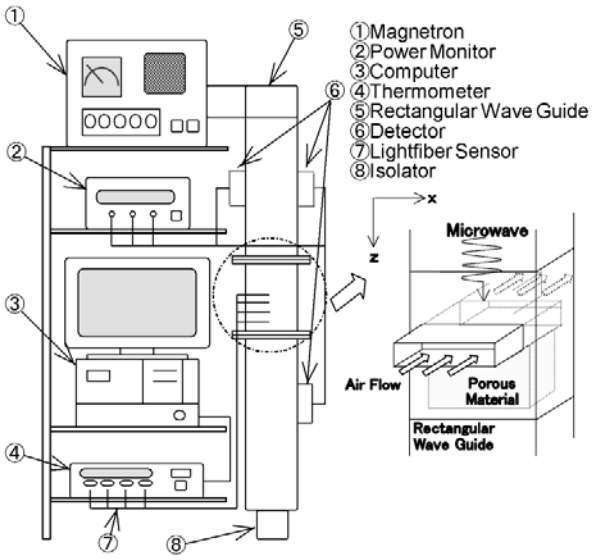

(a) Equipment list.

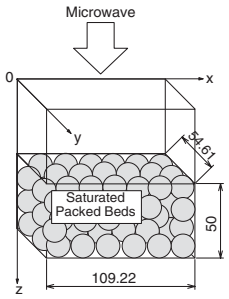

(b) Rectangular porous packed bed

Figure 1. Schematic diagram of the microwave drying system.

ANALYSIS OF MICROWAVE DRYING USING RECTANGULAR WAVE GUIDE

Generally, studies of microwave drying involve solutions of the equations governing electromagnetic propagation, i.e., Maxwell's equations, either by themselves or coupled with the heat and mass transport equations.

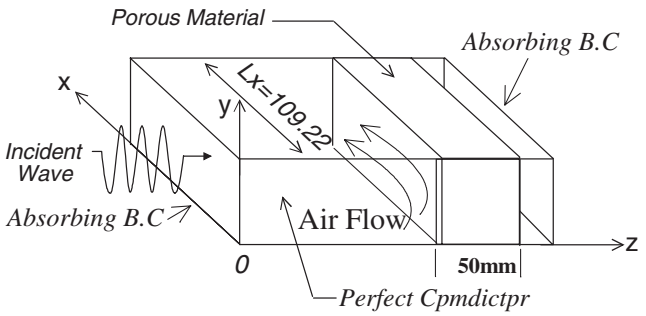

Figure 2. Analytical model.

The objective of this work is to understand the phenomena of heat and mass transport during microwave drying of capillary porous packed bed by using rectangular wave guide. A two-dimensional analytical model over the x–z plane in Figure 2 is presented. The surface of the sample is exposed to the external drying conditions. Microwave in the form of plane wave incident this surface. Other surfaces are insulated and the heat and moisture fluxes are set equal to zero.

Analysis of the Electromagnetic Field

Figure 2 shows the analytical model for microwave drying using a rectangular wave guide. The model proposed is based on the following assumptions:

1. Since the microwave field is of TE_{10} mode it propagates in a rectangular wave guide independently of the y-direction. Hence the electromagnetic field can be assumed to be two-dimensional in the x–z plane.
2. The absorption of microwave energy by the cavity (including air) in the rectangular wave guide is negligible.
3. The walls of a rectangular wave guide are perfect conductors.
4. The effect of the sample container on the electromagnetic field can be neglected.

The basic equations for the electromagnetic field are the well known Maxwell relations. When a microwave field propagates though an isotropic medium having permittivity ε, magnetic permeability μ, electric conductivity σ,

and electric charge density q, the governing equations are as follows;

$$\nabla \times \mathbf{E} = -\mu \frac{\partial \mathbf{H}}{\partial t} \tag{1}$$

$$\nabla \times \mathbf{H} = \sigma \mathbf{E} + \varepsilon \frac{\partial \mathbf{E}}{\partial t} \tag{2}$$

$$\nabla \cdot \mathbf{E} = \frac{q}{\varepsilon} \tag{3}$$

$$\nabla \cdot \mathbf{H} = 0 \tag{4}$$

For the microwave of TE_{10} mode, the components of electric and magnetic field intensities are given by

$$\begin{aligned} &E_x = E_z = H_y = 0 \\ &E_y, H_x, H_z \neq 0 \end{aligned} \tag{5}$$

where subscripts x, y and z represent x, y and z components of vectors, respectively. Taking into account Eq.(5), Eqs.(1)–(4) are written as, using the component notations of electric and magnetic field intensities,

$$\frac{\partial E_y}{\partial z} = \mu \frac{\partial H_x}{\partial t} \tag{6}$$

$$\frac{\partial E_y}{\partial x} = -\mu \frac{\partial H_z}{\partial t} \tag{7}$$

$$-\left(\frac{\partial H_z}{\partial x} - \frac{\partial H_x}{\partial z}\right) = \sigma E_y + \varepsilon \frac{\partial E_y}{\partial t} \tag{8}$$

where, permittivity ε, magnetic permeability μ and electric conductivity σ are given by

$$\varepsilon = \varepsilon_0 \varepsilon_r \tag{9}$$

$$\mu = \mu_0 \mu_r \tag{10}$$

$$\sigma = 2\pi f \varepsilon \tan\delta \tag{11}$$

where f is frequency of microwave, $\tan\delta$ is the dielectric loss coefficient, ε_r and μ_r are relative permittivity and relative magnetic permeability, respectively. Further, because the dielectric properties are assumed to vary with temperature and moisture content during the drying process, the dielectric properties utilized throughout this study use the Wagner equation which can be found in literature (Wang and Schmugge, 1990).

Corresponding to the analytical model shown in Figure 2, boundary conditions can be given as follows:

(a) Perfectly conducting boundaries

Boundary conditions on the inner wall surface of a rectangular wave guide are given using Faraday's law and Gauss' theorem, as

$$E_t = 0, \quad H_n = 0 \tag{12}$$

where subscripts t and n denote the components of tangential and normal directions, respectively.

(b) Continuity boundary condition

Boundary conditions along the interface between different materials, for example between air and dielectric material surface, are given as, using Ampere's law and Gauss theorem

$$\begin{aligned} E_t &= E_t^{'}, \quad H_t = H_t^{'} \\ D_n &= D_n^{'}, \quad B_n = B_n^{'} \end{aligned} \tag{13}$$

where $'$ denotes one of the different materials.

(c) Absorbing boundary condition

At both ends of the rectangular wave guide, the first order absorbing conditions proposed by Mur (1981) are applied.

$$\frac{\partial E_y}{\partial t} = \pm \upsilon \frac{\partial E_y}{\partial z} \tag{14}$$

Here, the symbol $\pm$ represents forward or backward waves and υ is phase velocity of the microwave.

(d) Oscillation of the electric and magnetic flied intensities by magnetron

Incident wave due to magnetron is given by the following equations.

$$E_y = E_{y\text{in}} \sin\left(\frac{\pi x}{L_x}\right) \sin(2\pi f t) \tag{15}$$

$$H_x = \frac{E_{y\text{in}}}{Z_H} \sin\left(\frac{\pi x}{L_x}\right) \sin(2\pi f t) \tag{16}$$

E_{yin} is the input value of electric field intensity, L_x is the length of rectangular wave guide in x-direction, Z_H is the wave impedance in cases where microwave propagates in rectangular wave guide, and can be represented by

$$Z_H = \frac{\lambda_g Z_I}{\lambda} = \frac{\lambda_g}{\lambda} \sqrt{\frac{\mu}{\varepsilon}} \tag{17}$$

where Z_I depends on material and is called intrinsic impedance. λ and λ_g are wave length of microwaves in free space and rectangular wave guide, respectively.

Analysis of Heat and Mass Transport

A schematic diagram of the model is shown in Figure 2. By conservation of mass and energy in the sample, the governing equation of mass and energy for all phases can be derived using the volume-averaging technique (Whitaker, 1977). The main transport mechanisms that enables moisture movement during microwave drying of the sample are: liquid flow driven by capillary pressure gradient and gravity while the vapor is driven by the gradient of the partial pressure of the evaporating species. The main assumptions involved in the formulation of the transport model are:

1. The capillary porous material is rigid. No chemical reactions occur in the sample.
2. Local thermodynamics equilibrium is assumed.
3. Simultaneous heat and mass transport occurs at constant pressure, where the dominant mechanisms are capillary transport, vapor diffusion and gravity. Such is generally the case in drying of capillary porous medium at atmospheric pressure when the temperature is lower than the boiling point (Bories, 1991).
4. The contribution of convection to energy transport is included.
5. Corresponding to electromagnetic field, temperature and moisture profiles also can be assumed to be two-dimensional in the x–z plane.
6. The effect of the sample container on temperature and moisture profiles can be neglected.

Mass Conservation

The microscopic mass conservation equations for liquid, water vapor, air, and gas phase, are written, respectively, as

$$\text{Liquid phase} \quad \rho_l \phi \frac{\partial s}{\partial t} + \rho_l \frac{\partial u_l}{\partial x} + \rho_l \frac{\partial w_l}{\partial z} = -\dot{n} \tag{18}$$

$$\text{Vapor phase} \quad \frac{\partial}{\partial t}\left\{\rho_v \phi (1-s)\right\} + \frac{\partial}{\partial x}[\rho_v u_v] + \frac{\partial}{\partial z}[\rho_v w_v] = \dot{n} \tag{19}$$

$$\text{Air phase} \quad \frac{\partial}{\partial t}\left\{\rho_a \phi (1-s)\right\} + \frac{\partial}{\partial x}[\rho_a u_a] + \frac{\partial}{\partial z}[\rho_a w_a] = 0 \tag{20}$$

$$\text{Gas phase} \quad \frac{\partial}{\partial t}\{\rho_g \phi(1-s)\} + \frac{\partial}{\partial x}[\rho_g u_g] + \frac{\partial}{\partial z}[\rho_g w_g] = \dot{n} \tag{21}$$

Here $\dot{n}$ is the evaporation rate during phase change and ϕ is the porosity of porous medium. The water vapor and air mass flux is the sum of the convective term with the gas superficial velocity and diffusive term.

Energy Conservation

Ignoring kinetic energy and pressure terms which are usually unimportant, this can be obtained from the total energy conservation for a combined solid, water vapor and air phase and by invoking the assumption that local thermodynamics equilibrium prevails among the all phases, the temperature of the sample exposed to irradiation is obtained by solving the conventional heat transport equation with the microwave power absorbed included as a local electromagnetic heat generation term. The governing energy equation describing the temperature rise in the sample is the time dependent equation is

$$\frac{\partial}{\partial t}[(\rho c_p)_T T] + \nabla[\{\rho_l c_{pl} u_l + (\rho_a c_{pa} + \rho_v c_{pv}) u_g\} T] + H_v \dot{n} = -\nabla q + Q \tag{22}$$

where Hv is the latent heat of vaporization of water and Q is the local electromagnetic heat generation term, which is a function of the electric field distribution and defined as

$$Q = 2\pi \cdot f \cdot \varepsilon_0 \cdot \varepsilon_r (\tan\delta) E_y^2 \tag{23}$$

where ε_r denotes relative dielectric constant, ε_0 denotes the permittivity of free space.

Phenomenological Relations

In order to complete the system of equations, the expressions for the superficial average velocity of the liquid and gas phases the generalized Darcy's law in the following form is used:

$$\vec{u}_l = -\frac{KK_{rl}}{\mu_l}[\nabla p_g - \nabla p_c - \rho_l \vec{g}] \tag{24}$$

$$\vec{u}_g = -\frac{KK_{rg}}{\mu_g}[\nabla p_g - \rho_g \vec{g}] \tag{25}$$

For the velocity of vapor water and air phase the generalized Fick's law for a two components gas mixture can be expressed as:

$$\rho_v \vec{u}_v = \rho_v \vec{u}_g - \rho_g D_m \nabla\left(\frac{\rho_v}{\rho_g}\right) \tag{26}$$

$$\rho_a \vec{u}_a = \rho_a \vec{u}_g - \rho_g D_m \nabla\left(\frac{\rho_a}{\rho_g}\right) \tag{27}$$

where the capillary pressure p_c is related to the gas and liquid phases can be written by

$$p_c = p_g - p_l \tag{28}$$

and D_m is the effective molecular mass diffusion (Rogers and Kaviany, 1992)

$$D_m = \frac{2\phi}{3-\phi}(1-s)D \tag{29}$$

where D is the binary mass diffusion in plain media.

Fourier's law is used to define the heat flux through the porous medium

$$q = -\lambda_{\text{eff}} \nabla T \tag{30}$$

Equilibrium Relations

The system of conservation equations obtained for multiphase transport mode requires constitutive equation for relative permeabilities K_r, capillary pressure p_c, capillary pressure functions (Leverett functions) J, and the effective thermal conductivity λ_{eff}. A typical set of constitutive relationships for liquid and gas system given by:

$$K_{rl} = s_e^3 \tag{31}$$

$$K_{rg} = (1 - s_e)^3 \tag{32}$$

where s_e is the effective water saturation considered the irreducible water saturation s_{ir} and defined by

$$s_e = \frac{s - s_{\text{ir}}}{1 - s_{\text{ir}}} \tag{33}$$

The capillary pressure p_c is further assumed to be adequately represented by Leverett's well known $J(s_e)$ functions. The relationship between

the capillary pressure and the water saturation is defined using Leverett functions $J(s_e)$:

$$p_c = p_g - p_l = \frac{\xi}{\sqrt{K/\phi}} J(s_e) \tag{34}$$

in which ξ is the gas-liquid interfacial tension. Aoki *et al.* (1991) correlated drainage capillary pressure data obtained by Leverett as follows to give $J(s_e)$:

$$J(s_e) = 0.325(1/s_e - 1)^{0.217} \tag{35}$$

The effective thermal conductivity of the capillary porous medium, λ, is also a function of water saturation which can be written as:

$$\lambda_{\text{eff}} = \frac{0.8}{1 + 3.78e^{-5.95s}} \tag{36}$$

State Equations

The gas phase is assumed to be an ideal mixture of perfect gases, so that the species density can be determined by the state equations, with the classical definitions for total density of the gas, ρ_g, and the mass average velocity of the gas:

$$\begin{aligned}
&\rho_a = \frac{p_a M_a}{R_o T}, \quad \rho_v = \frac{p_v M_v}{R_o T} \\
&\rho_g = \rho_a + \rho_v \\
&p_a = \rho_a R_a T, \quad p_v = \rho_v R_v T \\
&p_g = p_a + p_v \\
&\rho_g u_g = \rho_a u_a + \rho_v u_v
\end{aligned} \tag{37}$$

The partial pressure of the vapor was considered as a function of temperature (Watanuki, 1998) and defined by

$$p_v = C_0 + (C_1 + (C_2 + (C_3 + (C_4 + C_5 T)T)T)T)T \tag{38}$$

where

$$C_0 = 610.8,\ C_1 = 43.87,\ C_2 = 1.47,\ C_3 = 0.025,$$
$$C_4 = 2.88e - 4,\ C_5 = 2.71e - 6$$

Moisture Transport Equation

The phenomenon of moisture transport in the sample is described by the mass conservation equations for the liquid phase (equation 18) and the water vapor portion of the gas phase (equation 19) since it is the total water content that is of interest, these equations in two-dimensional scalar forms can be added together to yield an equation for the total moisture content as follows:

$$\phi\frac{\partial}{\partial t}\{\rho_l s+\rho_v(1-s)\}+\frac{\partial}{\partial x}[\rho_l u_l+\rho_v u_v]+\frac{\partial}{\partial z}[\rho_l w_l+\rho_v w_v]=0 \tag{39}$$

Using Darcy's generalized equation (equations 24,25) and Fick's law (equations. 26,27), the moisture transport equation is written as:

$$\begin{aligned}&\phi\frac{\partial}{\partial t}\{\rho_l s+\rho_v(1-s)\}+\frac{\partial}{\partial x}\left[\rho_l\frac{KK_{rl}}{\mu_g}\left(\frac{\partial p_c}{\partial x}-\frac{\partial p_g}{\partial x}+\rho_l g_x\right)\right.\\&\left.+\rho_v\frac{KK_{rg}}{\mu_l}\left(-\frac{\partial p_g}{\partial x}+\rho_g g_x\right)-D_m\frac{\partial\rho_v}{\partial x}\right]\\&+\frac{\partial}{\partial z}\left[\rho_l\frac{KK_{rl}}{\mu_l}\left(\frac{\partial p_c}{\partial z}-\frac{\partial p_g}{\partial z}+\rho_l g_z\right)+\rho_v\frac{KK_{rg}}{\mu_g}\left(-\frac{\partial p_g}{\partial z}+\rho_g g_z\right)-D_m\frac{\partial\rho_v}{\partial z}\right]=0\end{aligned} \tag{40}$$

In addition, it is assumed that the total pressure gradient ($p_g = \text{const}$) and gravitational effect in x-direction are negligible. Thus, equation (40) becomes

$$\begin{aligned}&\phi\frac{\partial}{\partial t}\{\rho_l s+\rho_v(1-s)\}+\frac{\partial}{\partial x}\left[\rho_l\frac{KK_{rl}}{\mu_l}\left(\frac{\partial p_c}{\partial x}\right)-D_m\frac{\partial\rho_v}{\partial x}\right]\\&+\frac{\partial}{\partial z}\left[\rho_l\frac{KK_{rl}}{\mu_l}\left(\frac{\partial p_c}{\partial z}+\rho_l g_z\right)+\rho_v\frac{KK_{rg}}{\mu_g}(\rho_g g_z)-D_m\frac{\partial\rho_v}{\partial z}\right]=0\end{aligned} \tag{41}$$

Heat Transport Equation

For a nonisothermal flow we must add temperature as a dependent variable. The conservation of energy equation for the two-dimensional model allows prediction of the temperature. Thus, equation (22) leads to:

$$\begin{aligned}&\frac{\partial}{\partial t}\left[(\rho c_p)_T T\right]+\frac{\partial}{\partial x}\left[\{\rho_l c_{pl}u_l+(\rho_a c_{pa}+\rho_v c_{pv})u_g\}T\right]+\\&\frac{\partial}{\partial z}\left[\{\rho_l c_{pl}w_l+(\rho_a c_{pa}+\rho_v c_{pv})w_g\}T\right]+H_v\dot{n}=\frac{\partial}{\partial x}\left[\lambda_{\text{eff}}\frac{\partial T}{\partial x}\right]+\frac{\partial}{\partial z}\left[\lambda_{\text{eff}}\frac{\partial T}{\partial z}\right]+Q\end{aligned} \tag{42}$$

where

$$(\rho c_p)_T = \rho_l c_{pl} \phi s + \{(\rho c_p)_a + (\rho c_p)_v\}\phi(1-s) + \rho_p c_{pp}(1-\phi) \tag{43}$$

$$\dot{n} = \frac{\partial}{\partial t}\{\rho_v \phi(1-s)\} + \frac{\partial}{\partial x}\left[-D_m \frac{\partial \rho_v}{\partial x}\right] + \frac{\partial}{\partial z}\left[\rho_v \frac{KK_{rg}}{\mu_g}\rho_g g_z - D_m \frac{\partial \rho_v}{\partial z}\right] \tag{44}$$

Boundary and Initial Conditions

There are two types of boundary conditions for solution of the governing equations are formulated at the open and impermeable boundaries.

The boundary conditions proposed for the open boundary of the sample, for the exchange of energy at the open boundary can be described in the following form:

$$-\lambda_{\text{eff}} \frac{\partial T}{\partial z} = h_c(T - T_\infty) + n H_v \tag{45}$$

where h_c is the local heat transfer coefficient.

Mass transfer at the open boundary is modeled by means of a locally constant mass transfer coefficient, which is related to the local water vapor flux density is described as:

$$\rho_l w_l + \rho_v w_v = h_{ms}(\rho_{vs} - \rho_{v\infty}) \tag{46}$$

where h_{ms} is the local mass transfer coefficient, ρ_{vs} is the density of water vapor at the open boundary and $\rho_{v\infty}$ is reference vapor density in the gas phase surrounding the open boundary. Considering the boundary conditions at the closed boundary (symmetry-impermeable) that no heat and mass exchange take place:

$$\frac{\partial T}{\partial x} = \frac{\partial T}{\partial z} = 0 \tag{47}$$

$$\frac{\partial u}{\partial x} = \frac{\partial w}{\partial z} = 0 \tag{48}$$

The initial conditions are uniform initial temperature and moisture.

Numerical Procedure

In order to predict the electromagnetic field, a finite difference time domain (FDTD) method is applied (Yee, 1966). The system of nonlinear

partial differential equations (Equations. (41)–(48)) must be solved by the method of finite differences based on the notion of control volumes as described by Patankar (1980). At each time increment, the nodal value of s and T were solved iteratively and convergence was checked on both variables. The Newton-Raphson method was employed at each iteration to quicker the convergence. Initially, the temperature and moisture profiles were set to be equal at all nodes at values corresponding to the measured capillary porous medium conditions. Since the propagating velocity of microwave is very fast compared with the rates of heat and mass transfer, different time steps of $dt = 4$ [ps] and 1[s] are used for the computation of the electromagnetic field and temperature and moisture profile calculations. The spatial step size is $dx = dz = 1$[mm]. Some of the input data for electromagnetic and thermo physical properties and drying conditions are given in Table 1 and Table 2, respectively.

RESULTS AND DISCUSSION

The experimental results for microwave drying of a capillary porous packed bed (glass beads + water) were compared with mathematical model

Table 1. The Electromagnetic and Thermo Physical Properties Used in the Computations

$\varepsilon_0 = 8.85419 \times 10^{-12}$[F/m],	$\mu_0 = 4.0\pi \times 10^{-7}$[H/m]	
$\varepsilon_{\mathrm{ra}} = 1.0$,	$\varepsilon_{\mathrm{rp}} = 5.1$	
$\mu_{\mathrm{ra}} = 1.0$,	$\mu_{\mathrm{rp}} = 1.0$,	$\mu_{rl} = 1.0$
$\tan\delta_a = 0.0$,	$\tan\delta_p = 0.01$	
$\rho_a = 1.205$ [kg/m^3],	$\rho_p = 2500.0$ [kg/m^3],	$\rho_l = 1000.0$ [kg/m^3]
$c_{pa} = 1.007$ [kJ/(kg · K)],	$c_{pp} = 0.80$ [kJ/(kg · K)],	$c_{pl} = 4.186$ [kJ/(kg · K)]

Table 2. The Drying Conditions Used in the Computations

Drying Conditions	Value
Glass bead size, d [mm]	0.15, 0.4
Initial saturation, So [−]	0.99
Initial temperature, To [°C]	12
Irreducible saturation, S_{ir} [−]	0.06
Porosity, ϕ [−]	0.385, 0.371
Air velocity, U_∞ (m/s)	7.2
Surrounding temperature, T_∞ [°C]	12

simulations. In order to test the validity of the mathematical model, the results are divided into three parts that cover, on the part one is the simulation of electric field in a rectangular wave guide and sample. Part two shows the results of the distribution of temperature and moisture profiles in the sample. The third part shows the general observation of graphical results during drying. However, all processes using the two levels of microwave power input ($P = 50\,\mathrm{W}$, $P = 100\,\mathrm{W}$) were distinguished. One aspect of model verification was to compare drying data from experiments run under different conditions with mathematical simulations using parameter values obtained from Table 1 and Table 2.

Simulation of the Electric Field in a Rectangular Wave Guide

To understand the electrical field inside the rectangular wave guide and the sample, simulation analysis is required. In figures 3 and 4 are the simulated the electric field of TE_{10} mode along the center axis $x = 54.61$ of rectangular wave guide, for the case of a rectangular wave guide is empty (which corresponds to that of air) and for the case when the sample is inserted in the rectangular wave guide, respectively. The vertical axis represents the intensity of the electric field E_y, which is normalized to the amplitude of the input electromagnetic wave, E_{yin}. Figure 3 shows the standing wave of TE_{10} mode, for the case of a rectangular wave guide is empty. A uniform static wave is formed inside a rectangular wave guide. In Figure 4 corresponding to the case when the sample is inserted in the rectangular

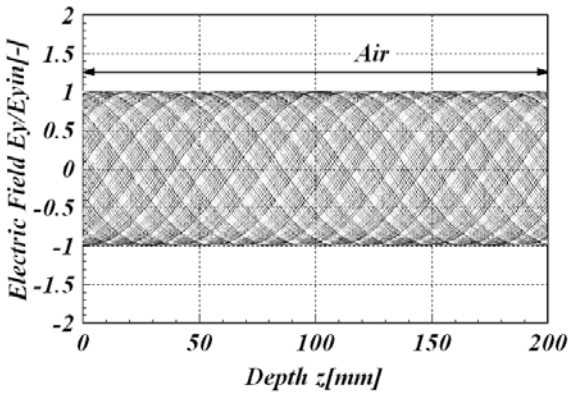

Figure 3. Distribution of electric field along the center axis for case of a rectangular wave guide is empty.

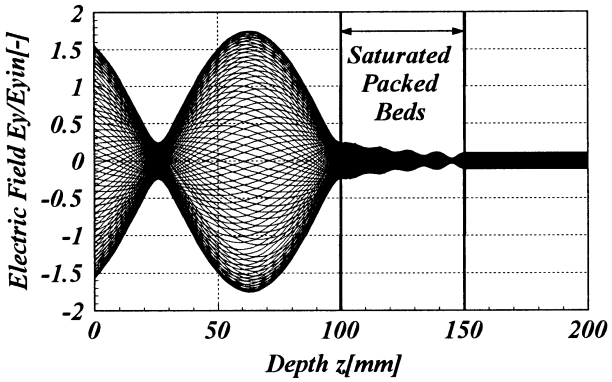

Figure 4. Distribution of electric field along the center axis for the sample is inserted in the rectangular wave guide ($t = 1$ min).

wave guide, since the incident wave passing through the cavity having low permittivity is directly irradiated to the sample having high permittivity, a major part of incident wave is reflected on the surface of the sample and the standing waves form in the cavity forward to the sample. In early stage of drying, it is found that the electric field distribution within the sample are almost extinguished. On the other hand, the electric field distribution for the end stage of drying process, in which case after a majority of the moisture level inside the sample is decreased, the effect of reflection rate on the surface of the sample is lower which increases the penetration depth of the microwave inside the sample.

Distribution of Temperature and Moisture Profiles Within the Sample

Mathematical model simulation results are compared with experimental microwave drying data in Figures 5 through 11.

The temperature profile as a function of distance at various times for a microwave power level of 100 W are shown in Figure 5, which correspond to those of initial temperature with 12°C, along with the center axis $x = 54.61$ mm of rectangular wave guide. In contrast to that in conventional drying, microwave drying gives higher temperatures inside the drying sample while the surface temperature stays colder due to the cooling effect of surrounding air. At the same time the evaporation takes place at the

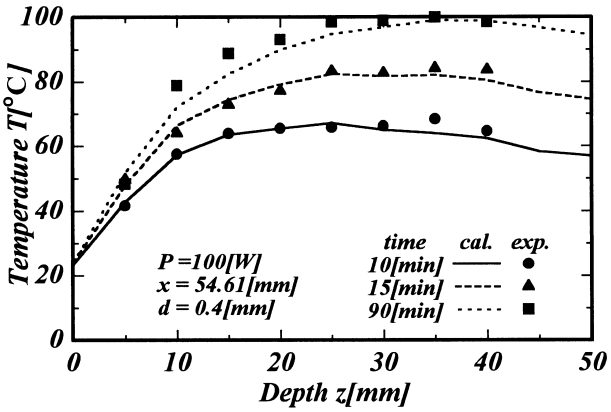

Figure 5. Temperature as a function of distance at various times ($P = 100$ W, $d = 0.4$ mm, $x = 54.61$ mm).

surface of the sample at a lower temperature due to evaporative cooling. The simulated results are in agreement with the experimental results for microwave drying.

The temperature profiles at various times and at various distances are shown in Figures 6 and 7. Figure 6 shows that the temperature profile within the sample rises up quickly in the early stage of the drying process, after that its rise slows down. In Figure 6, near the end stage of drying as the moisture content inside the sample is reduced, this decreases the microwave power absorbed resulting in a lower sample temperature. However, at a high microwave power input (100 W) as shown in Figure 7, the temperature profile within the sample continuously rises faster than that in the case of low microwave power input (50 W). Also, the temperature remains high at the end of drying. The simulated results are in good agreement with the experimental results.

The following discussion refers to the effect of glass bead size under same conditions. The temperature and moisture profiles are shown in Figures 8–11. Figure 8 shows the temperature profiles for two sizes ($d = 0.15$ mm and $d = 0.4$ mm). The observed temperature profiles at the leading edge of the sample in the case of small glass bead size are higher than those in the case of larger size beads. This is because of the small glass bead size (which corresponds to a higher capillary force) can cause moisture to reach the surface at a higher rate than that in the case of larger bead size (see Figure 10); this corresponds to a greater amount of microwave power absorbed. Hence, even higher moisture content can lead to higher

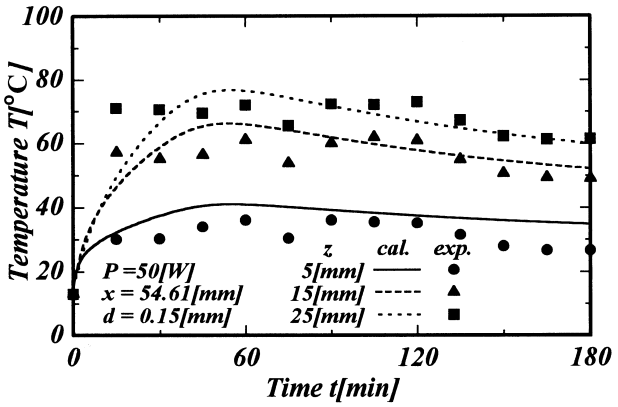

Figure 6. Temperature profile in times at various distances ($P = 50$ W, $d = 0.15$ mm, $x = 54.61$ mm).

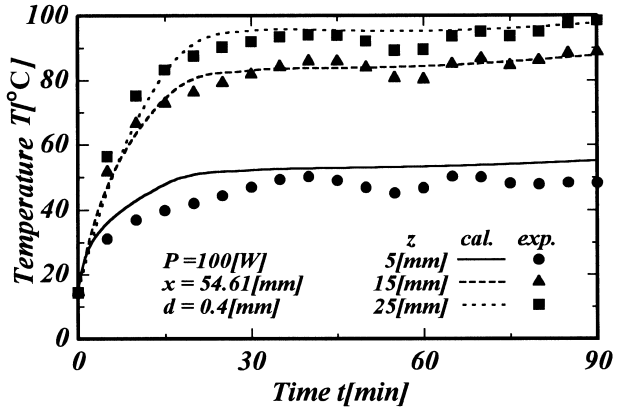

Figure 7. Temperature profile in times at various distances ($P = 100$ W, $d = 0.4$ mm, $x = 54.61$ mm).

temperatures in this region. On the other hand, for the case of the smaller bead size, the temperature profile deep inside the sample is still lower due to the lower of moisture as well as microwave power absorbed inside the sample. Continued drying would eventually cause the average moisture content inside the sample to decrease and lead to decreased microwave power absorbed, reduced temperature inside the sample; this is more significant in the case of smaller bead size (Figure 9).

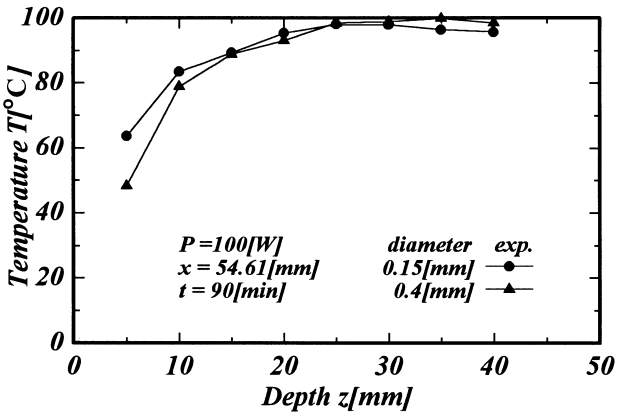

Figure 8. Comparison temperature as a function of distance ($P = 100$ W, $t = 90$ min, $x = 54.61$ mm).

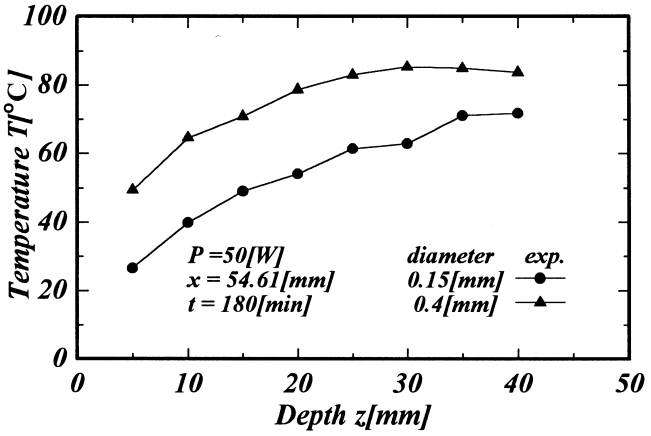

Figure 9. Comparison temperature as a function of distance ($P = 50$ W, $t = 180$ min, $x = 54.61$ mm).

The variation of the drying rate with time obtained by simulation is compared with the experimental results in Figure 11. The small bead size, however, leads to much higher capillary forces resulting in a shorter drying time and more uniform moisture profile inside the sample. The simulated results are in good agreement with the experimental results.

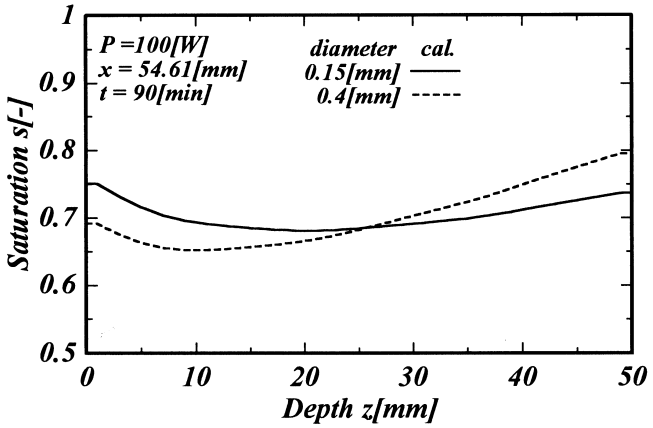

Figure 10. Comparison water saturation as a function of distance ($P = 100$ W, $t = 90$ min, $x = 54.61$ mm).

General Observations on the Graphical Results During Microwave Drying Process

The simulation results presented in the form of three-dimensional surface plots are considered in here. Figure 12 shows that in the early stages of drying, the temperature in the sample closest to the incoming microwave and the distribution of temperature has a wavy shape corresponding to that of electromagnetic field. This region heats up to a higher level at a faster rate than elsewhere in the sample. Figure 13 shows that as the temperature inside rises to a higher level, the evaporation rate increases and the moisture is driven quickly toward the surface where it evaporates and cools the surface. Figures 14 and 15 show the simulated moisture distributions within the sample for a microwave power input of 100 W. Figure 14 shows that in the early stages of the drying process, the moisture content at the leading edge of the sample is lower than that inside the sample, where the moisture decreases due to the gravitational effect. Because of the higher moisture content much larger reflected waves develop at the surface during the early stages of the drying process. Later, the surface of the sample is supplied with liquid water through gradient in the capillary pressure, and because of the condensation of water vapor (which moves towards the surface due to a gradient in the vapor partial pressure), due to the lower temperature of the surface. In Figure 15, continued drying would eventually cause the average moisture content inside the sample to decrease and lead to decreased microwave power absorbed, reduced temperature and evapora-

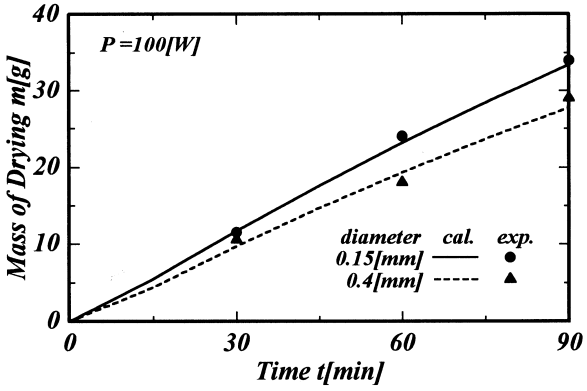

(a)

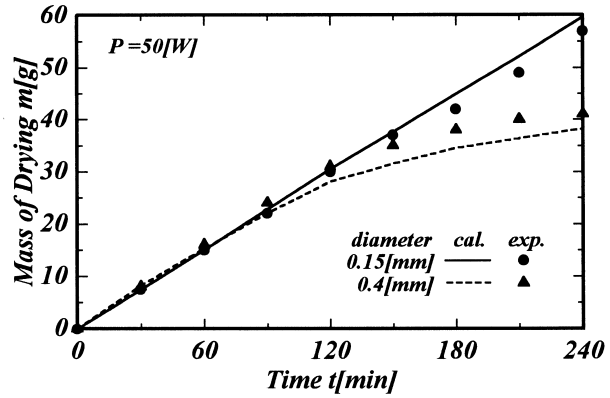

(b)

Figure 11. The variation of drying rate with respect to time at (a) microwave power input, $P = 100$ W, (b) microwave power input, $P = 50$ W.

tion rate. However, at longer times, the capillary pressure continues to push inside the moisture to accumulate at the surface and it is slightly higher than that observed for moisture content inside the sample, especially, for the case of small glass bead size (Figure 10). Nevertheless, the moisture content now appears higher close to the walls of the sample.

Due to the large initial moisture content, the skin-depth heating effect causes a major part of the incident wave to be reflected from the surface

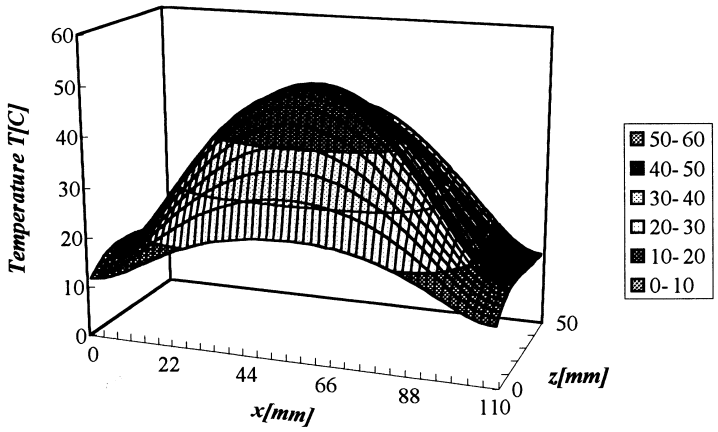

Figure 12. Carpet plot of temperature distributions ($t = 9$ min, $P = 100$ W).

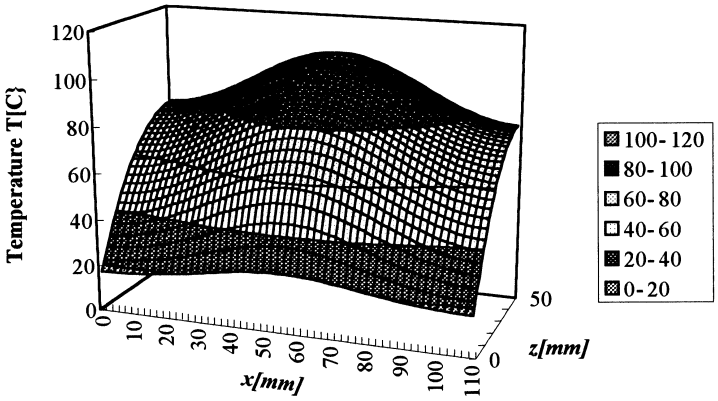

Figure 13. Carpet plot of temperature distributions ($t = 90$ min, $P = 100$ W).

during the early stages of drying. This phenomenon explains why the amplitude of microwave within the sample in the early stage of drying is slightly lower than that observed in the final stage of drying and why the heating is more intense close to the leading edge of the sample. Perre and Turner, (1997) reached the same conclusion for this phenomenon. However, continued drying eventually causes the average moisture content inside the sample to decrease; the larger part of the microwave can then penetrate further into the sample compared with the early stage of drying.

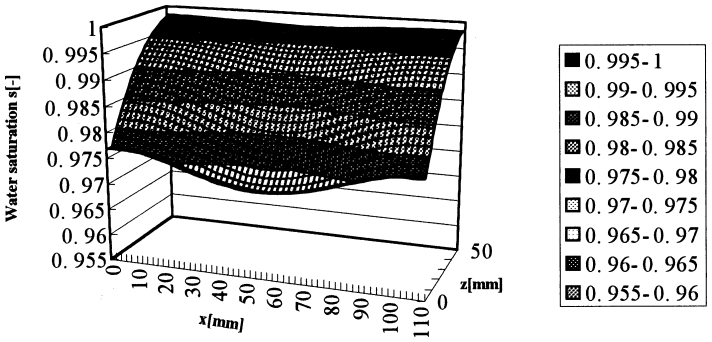

Figure 14. Carpet plot of moisture distributions ($t = 9$ min, $P = 100$ W).

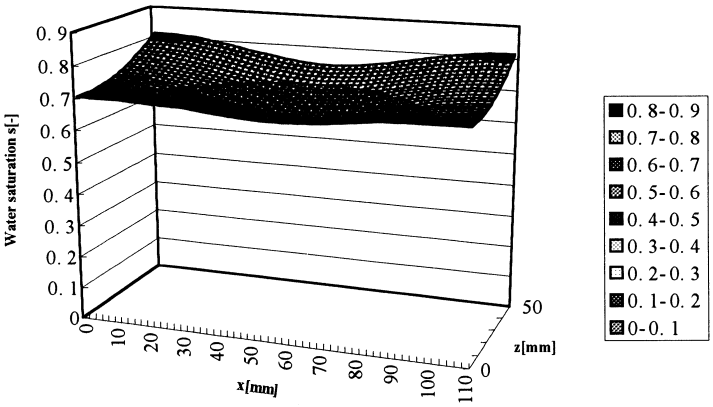

Figure 15. Carpet plot of moisture distributions ($t = 90$ min, $P = 100$ W).

CONCLUSIONS

The experiments and theoretically analysis presented in this paper-describe many of the important interactions within a capillary porous medium during microwave drying using a rectangular wave guide. The following summarizes the conclusions of this work:

1) A generalized mathematical model of drying by microwave using rectangular wave guide is proposed. It is used successfully to describe the drying phenomena under various conditions.

2) The calculations of electromagnetic fields inside the rectangular wave guide and the sample show that the variation of microwave power level and glass size changes the degree of penetration and rate of heat generation within the sample. The reflection rate of microwave strongly depends on the amount of moisture content within the sample.
3) The small bead size leads to much higher capillary forces resulting in a faster drying time.
4) At the longer drying times that the drying phenomenon is very complicated for the theoretical explanation, in situation where the materials dry at certain locations and absorb microwave radiation more efficiently at higher temperature due to dramatic increases in dielectric loss coefficient, a local exponential rise in temperature can occur. This phenomenon, commonly referred to as thermal runaway effect. Consequently, the dielectric properties database must be carefully used in the computational procedure. See Ratanadecho *et al.* (2001) for a detail discussion.

NOMENCLATURE

C_p	Specific heat capacity [J/kgK]
E	Electric field intensity [V/m]
g	Gravitational constant [m/s^2]
H	Magnetic field intensity [A/m]
P	Microwave power input [W]
Q	Heat generation [W/m^3]
R	Universal gas constant [J/mol/K]
s	Water saturation [–]
T	Temperature [ ]
t	Time [s]
u	Velocity [m/s]
K	Permeability [m^2]
M	Molecular weight [kg/kg-mol]
p	Pressure [Pa]
w	Velocity [m/s]

Greek letters

ϕ	Porosity [m^3/m^3]
ρ	Density [kg/m^3]
ε	Permittivity [F/m]

λ	Free space wave length [m]
μ	Magnetic permeability [H/m]
υ	Velocity of propagation [m/s]
λ_{eff}	Effective conductivity [W/mK]
μ_g	Dynamic viscosity of gas [Pa s]
μ_l	Dynamic viscosity of liquid [Pa s]

Subscripts

0	Free space
a	Air
c	Capillary
g	Gas
p	Particle
r	Relative
v	Water vapor
l	Liquid water
x, y, z	Coordinates

REFERENCES

1. Aoki, K., Hattori, M., Kitamura, M. and Shiraishi, N., 1991, Characteristics of heat Transport in Porous Media with Water Infiltration, *ASME/JSME Thermal Engineering Proceedings*, Vol. 4, pp. 303–308.
2. Bories, S.A., 1991, Fundamental of drying of capillary-porous bodies, pp. 39–434, in Kakac, S., Kilkis, B., Kulacki, F. and Arinc, F. (Ed.), *Convective heat and mass transfer in porous media. NATO ASI series*, Vol. 196, Kluwer Publishers.
3. Constant, T., Moyne, C. and Perre, P., 1996, Drying with internal heat generation: Theoretical aspects and application to microwave heating, *AIChE J.*, 42 (2) pp. 359–368.
4. Mur, G., 1981, Absorbing boundary conditions for the Finite-Difference Approximation of the Time-Domain Electromagnetic-Field Equations, *IEEE Transactions of Electromagnetic Compatibility*, EMC-23 (4) pp. 377–382.
5. Metaxas, A.C. and Meridith, R.J., 1983, *Industrial Microwave Heating*, Peter Peregrinus, Ltd., London.
6. Mujumdar, A.S. (Ed.), 1995, *Handbook of Industrial Drying, 2nd Edition*, Marcel Dekker, New York.

7. Ni, H., Datta, A. and Torrance, K.E., 1999, Moisture transport in intensive microwave heating of biomaterials: a multiphase porous media model, *Int. J. Heat and Mass Transfer*, 42 (8) pp. 1501–1512.
8. Perre, P. and Turner, W., 1997, Microwave Drying of softwood in an Oversized Waveguide, *AIChE J.*, 43 (10) pp. 2579–2595.
9. Patankar, S.V., 1980 *Numerical Heat Transfer and Fluid Flow*, Hemisphere Publishing Corporation, New York.
10. Rogers, J.A. and Kaviany, M., 1992, Funicular and evaporative-front regimes in convective drying of granular beds, *Int. J. Heat and Mass Transfer*, 35 (2) pp. 469–479.
11. Ratanadecho, P., Aoki, K. and Akahori, M., 2001, Experimental and numerical study of microwave drying in unsaturated porous material, *Int. Communication. Heat Mass Trans*, Vol 28 (5), pp. 605–616.
12. Ratandecho, P., Aoki, K. and Akahori, M., 2001, Influence of irradiation time, particle sizes and initial moisture content during microwave drying of multi-layered capillary porous materials, *ASME J. Heat Transfer* (to be published).
13. Saltiel, C. and Datta, A., 1990, Heat and mass transfer in microwave processing, *Adv. Heat Transfer*, pp. 3–15.
14. Turner, I.W. and Jolly, P.G., 1990, The effect of dielectric properties on microwave drying kinetics, *J. Microwave power and electromagnetic energy*, 25 (1) 30 (4) pp. 221–223.
15. Turner, I.W. and Jolly, P.G., 1991, Combined microwave and convective drying of a porous material, *Drying Technology*, 9 (5) pp. 1209–1269.
16. Von Hippel, A.R., 1954, *Dielectric Materials and Applications*, MIT Press, Boston.
17. Wei, C.K., Davis, H.T., Davis, E.A. and Gordon, J., 1985, Heat and mass transfer in water-laden sand stone: microwave heating, *AIChE J.*, 31 (5) pp. 842–848.
18. Watanuki, J., 1998, *Fundamental study of Microwave Heating with Rectangular Wave guide*, M.S. Thesis (In Japanese), Nagaoka University of Technology, Japan 85 p.
19. Wang, J. and Schmugge, T., 1980, An empirical model for the complex dielectric permittivity of soil as a function of water content, *IEEE Transactions on Geosciences and Remote Sensing*, GE-18 (4) pp. 288–295.
20. Whitaker, S., 1977, A theory of drying in porous media, *Adv. Heat Transfer* (13), pp. 119–203.
21. Yee, K.S., 1966, Numerical solution of initial boundary value problems involving Maxwell's equation in isotropic media, *IEEE Transactions of Antennas Propagation*, AP-14 pp. 302–307.